

Ferromagnetism in the Mott insulator  $\text{Ba}_2\text{NaO}_5\text{SO}_6$ A. S. Erickson,<sup>1</sup> S. M. Isra,<sup>2</sup> G. J. Miller,<sup>2</sup> R. R. Gupta,<sup>3</sup> Z. Schlesinger,<sup>3</sup> W. A. Harrison,<sup>1</sup> J. M. Kim,<sup>1</sup> I. R. Fisher<sup>1</sup><sup>1</sup> Department of Applied Physics and Geballe Laboratory for Advanced Materials, Stanford University, CA 94305.<sup>2</sup> Department of Chemistry and Ames Laboratory, Iowa State University, Ames, IA 50011-2300<sup>3</sup> Department of Physics, University of California, Santa Cruz, CA 95064

Dated: February 8, 2020

Results are presented of single crystal structural, thermodynamic, and resistivity measurements of the double-perovskite  $\text{Ba}_2\text{NaO}_5\text{SO}_6$  that characterize the material as a  $5d^1$  ferromagnetic Mott insulator with an ordered moment of  $0.2 \mu_B$  per formula unit and  $T_C = 6.8(3)$  K. The implications of the coexistence of ferromagnetism and Mott insulation on the orbital state are discussed, and it is suggested that the ferromagnetism stems from ordering of the  $\text{O}_5\text{SO}_6$   $t_{2g}$  molecular orbitals.

PACS numbers: 75.50.Dd, 75.30.Cr, 71.70.Ej

The interplay between spin, orbital, and charge degrees of freedom in 3d transition metal oxides has proven to be a rich area of research in recent years. Despite the wide array of interesting physics found in these materials, much less is known about whether similar behavior can be found in related 4d and 5d systems, for which both the extent of the d-orbitals and larger spin-orbit coupling cause a different balance between the relevant energy scales. In this respect, oxides of osmium are of particular interest because the element can take formal valences from  $4+$  to  $7+$ , corresponding to electron configurations  $5d^4$  to  $5d^1$ . In this instance, we examine the simplest case of a  $5d^1$  osmate for which we find evidence that orbital ordering influences the magnetic structure.

Simple oxides of osmium are typically Pauli paramagnets due to the large extent of the 5d orbitals. Examples include the binary oxide  $\text{O}_5\text{S}\text{O}_2$  [1, 2] and the simple perovskites  $\text{AO}_5\text{O}_3$  ( $\text{A} = \text{Sr}, \text{Ba}$ ) [3]. However, more complex oxides, including the double and triple perovskites  $\text{La}_2\text{NaO}_5\text{SO}_6$  [4],  $\text{Ba}_2\text{AO}_5\text{SO}_6$  ( $\text{A} = \text{Li}, \text{Na}$ ) [5, 6] and  $\text{Ba}_3\text{AO}_5\text{S}_2\text{O}_9$ , ( $\text{A} = \text{Li}, \text{Na}$ ) [7], appear to exhibit local moment behavior. Presumably the large separation of O<sup>2-</sup> ions in these more complex structures leads to a Mott insulating state, and indeed these and related materials are most often found to be antiferromagnetic.

Of the above oxides and their near relations containing no other magnetic ions,  $\text{Ba}_2\text{NaO}_5\text{SO}_6$  distinguishes itself as the only material with a substantial ferromagnetic moment ( $0.2 \mu_B$ ) in the ordered state [5]. Given the low value of this moment and the tendency towards antiferromagnetism in related oxides, it would be natural to suggest that this moment arises from a canted antiferromagnetic structure. However the room temperature crystal structure of the material has an undistorted double-perovskite structure (Fig. 1(a)), space group  $\text{Fm}\bar{3}\text{m}$  [5], in which  $\text{O}_5\text{SO}_6$  octahedra are neither distorted nor rotated with respect to each other or the underlying lattice. Such a high crystal symmetry, if preserved to low temperatures, precludes the more usual mechanisms for obtaining a small ferromagnetic moment in a canted antiferromagnet [8], suggesting that a different

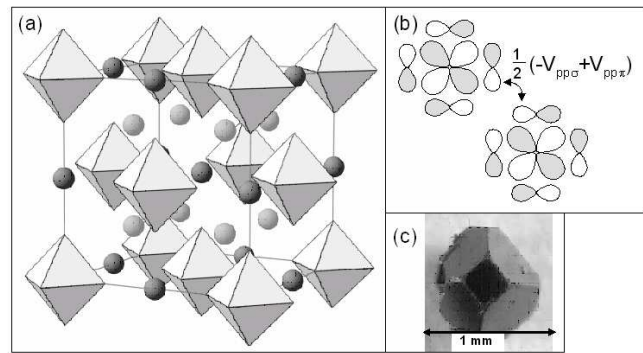


FIG. 1: (a) Double perovskite crystal structure of  $\text{Ba}_2\text{NaO}_5\text{SO}_6$ , illustrating the  $\text{O}_5\text{SO}_6$  octahedra central to the electronic structure.  $\text{Ba}$  and  $\text{Na}$  atoms are shown as dark and light grey spheres respectively. (b) Schematic diagram showing the coupling between two adjacent  $\text{O}_5\text{SO}_6$  molecular orbitals with  $d_{xy}$  symmetry for  $\mathbf{k} = 0$ . (c) Typical crystal seen along the [100] direction.

mechanism is causing the ferromagnetism.

In this paper we report measurements of the temperature dependence of the crystal structure, electrical resistivity, optical resistivity, magnetization, and heat capacity of single crystals of  $\text{Ba}_2\text{NaO}_5\text{SO}_6$ . We find that the material is a Mott insulator, and that there are no observable changes in the crystal structure down to temperatures below  $T_C = 6.8(3)$  K. These data suggest that the ferromagnetism is intrinsic in this material, placing it in the novel class of materials such as  $\text{YTb}_3$  [9, 10], in which the ferromagnetism is derived from ordering of the d orbitals, and is intimately linked to the presence of the Mott insulating state.

$\text{Ba}_2\text{NaO}_5\text{SO}_6$  was first synthesized in polycrystalline form by Sleight et. al. [6], and later in single crystal form by Stitzer and co-workers [5]. Single crystals for this study were grown following a method similar to that presented in reference [6]. Elementals  $\text{Ba(OH)}_2 \cdot 8\text{H}_2\text{O}$  and  $\text{NaOH}$  were mixed in the ratio 1:2.1:100, heated to 600 C over a period of 12 hrs in a covered 20 ml alumina crucible, and held at this temperature for 4-5 days. The

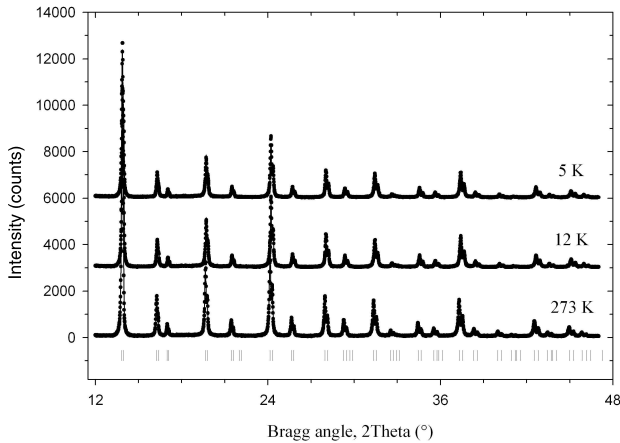


FIG. 2: Observed (dots) and calculated (line) X-ray powder diffraction patterns of  $\text{Ba}_2\text{Na}_0.5\text{SO}_6$  collected at 273, 12 and 5 K. Vertical bars under the observed and calculated diffraction patterns indicate calculated positions of Bragg peaks.

furnace was turned off when all of the flux had evaporated. Shiny, black, single crystals up to 2 mm in diameter with a truncated octahedral morphology (Fig. 1(c)) were picked from the crucible and washed in methanol.

Single crystal x-ray diffraction data were collected at room temperature using both a STOE Image Plate Diffractometer (IPDS II) and a Bruker Smart Apex CCD diffractometer. Data were taken for a crystal with dimensions 0.23 × 0.18 × 0.01 mm<sup>3</sup>, and for a smaller piece broken from this larger crystal with dimensions 0.058 × 0.039 × 0.022 mm<sup>3</sup>, more closely approximating a sphere. In each case, a large number of reflections were collected (3074 and 2166 respectively), and the structure was refined using the SHELXTL package of crystallographic programs [11]. Results could not be distinguished from fully occupied, stoichiometric  $\text{Ba}_2\text{Na}_0.5\text{SO}_6$  with the undistorted Fm 3m structure previously reported [5]. These measurements were repeated at temperatures of 243, 223, 198, and 183 K, with no difference in the refined structures. Additional powder diffraction measurements were taken at temperatures of 273, 30, 12 and 5 K (Fig. 2), using a Rigaku TTRAX powder diffractometer, equipped with a helium-flow cryostat. The structure was obtained by Rietveld refinement using the Rietica LHPM software [12]. No distortion from the double perovskite crystal structure was detected within the resolution of the measurement at any temperature.

With one electron per osmium site, one might naively expect metallic conductivity in this system. DC resistivity measurements consistently showed insulating behavior, but concern over the quality of the electrical contact to the samples led us to verify this observation by infrared reflectivity. Measurements were carried out using a scanning Fourier transform interferometer with a

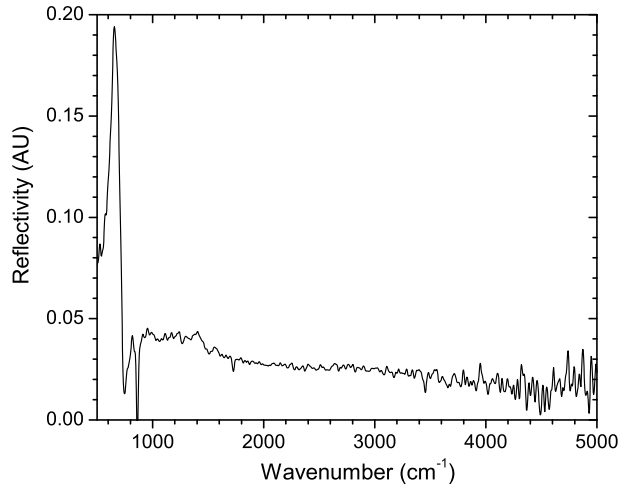


FIG. 3: IR reflectivity data as a function of wavenumber for  $\text{Ba}_2\text{Na}_0.5\text{SO}_6$ .

bolometer detector at 4.2 K, for arbitrary crystal orientations with the sample held at room temperature (Fig. 3). An evaporated Ag film, adjacent to and co-planar with the sample, provided a reference used to obtain absolute reflectivity versus frequency [13]. The data show low overall reflectivity, with no indication of a metallic plasmon edge down to the lowest measured frequency of 400 cm<sup>-1</sup>. The strong variations in the reflectivity between 400 and 1000 cm<sup>-1</sup> are a signature of unscreened optical phonons. These data suggest that  $\text{Ba}_2\text{Na}_0.5\text{SO}_6$  is a Mott insulator, which is supported by the following tight-binding analysis.

The crystal structure of  $\text{Ba}_2\text{Na}_0.5\text{SO}_6$  can be pictured as an FCC lattice of isolated  $\text{SO}_6$  octahedra separated by Ba and Na ions (Fig 1(a)). The s orbitals of Ba and Na are so high in energy that they can be neglected, and the electronic structure is primarily determined by the  $\text{SO}_6$  octahedra, which form the usual set of molecular orbitals. The bonding and non-bonding states are filled, leaving one electron in the triply-degenerate  $t_{2g}$  antibonding orbitals. Using the known energies for the O s and O p orbitals we find that this molecular orbital is at -13.43 eV [14], relative to  $E_p(\text{O}) = -16.77$  eV for oxygen 2p states and  $E_d(\text{O}) = -16.32$  eV [20]. Since the O s d and O p orbitals are close in energy, these molecular orbitals have almost equal 5d and 2p character.

Adjacent  $\text{SO}_6$  octahedra in  $\text{Ba}_2\text{Na}_0.5\text{SO}_6$  are coupled by the matrix elements  $\frac{1}{2}(-V_{pp} + V_{pp}')$  (Fig 1(b)). Using values obtained for similar cluster separations in other materials [14], modified appropriately for this particular lattice, and neglecting spin-orbit coupling, we obtain  $t = 1=4 \quad 1=2 (V_p + V_{pp}') = 0.05$  eV for the hopping matrix elements coupling adjacent octahedra. In

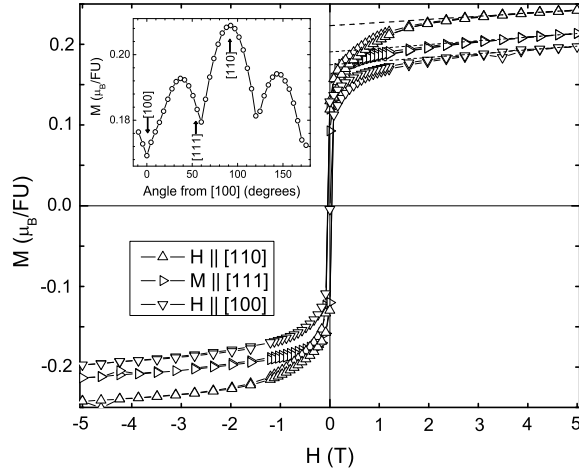


FIG. 4: Magnetization of  $\text{Ba}_2\text{Na}_0.5\text{SO}_6$  along high symmetry directions as a function of applied field at 1.8 K for a full hysteresis loop. 'FU' refers to one formula unit. Inset shows magnetization as a function of angle in the (011) plane at a temperature of 1.8 K and a field of 2 T. A line is drawn between data points to guide the eye.

contrast, the Coulomb energy associated with moving one electron from an  $\text{O}\text{SO}_6$  octahedron to its neighbor is found to be  $U = 3.3 \text{ eV}$  [21]. More detailed treatments could presumably refine these values, but since we find  $U \ll t$  it is clear that the material is a Mott insulator.

Magnetization measurements as a function of applied field at 1.8 K (Fig. 4) show ferromagnetic behavior, as previously reported for polycrystalline samples [5]. These data were obtained for applied fields oriented along high symmetry directions using a Quantum Design Superconducting Quantum Interference Device magnetometer for single crystals weighing between 2 and 7 mg. The magnetization rises rapidly in low fields and levels off for fields above 1 T, beyond which there is no discernable hysteresis. However, the absolute value of the magnetization at this field is relatively small (approximately  $0.2 \mu_B$ ) and does not appear to saturate up to fields of 5 T. Extrapolating a linear fit to the magnetization between 3 and 5 T, we obtain a zero-field magnetization of  $0.175(2)$ ,  $0.191(1)$ , and  $0.223(1) \mu_B$  for fields oriented along [100], [111], and [110], respectively. This anisotropy is confirmed by angle-dependent measurements at a constant field using a rotating sample holder and rotating in the (011) plane, which contains all three high-symmetry directions (inset to Fig. 4).

Temperature-dependent magnetization measurements in fields above 1 T, for which there is no hysteresis, show an upturn below approximately 8 K (Fig. 5), consistent with ferromagnetic behavior. The inverse susceptibility at high temperature shows a moderate amount of curva-

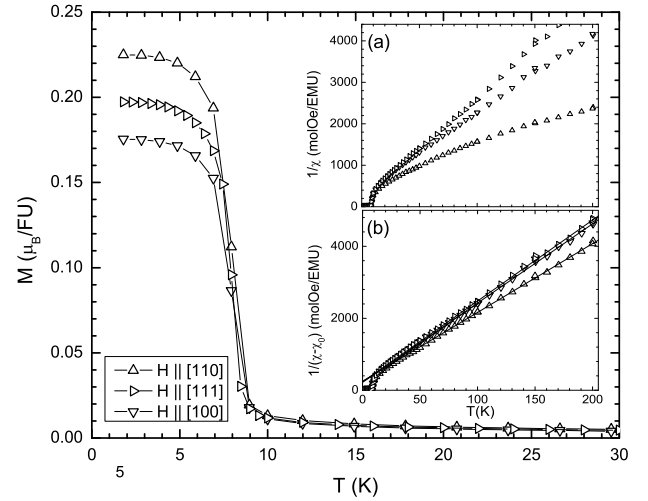


FIG. 5: Low temperature magnetization of  $\text{Ba}_2\text{Na}_0.5\text{SO}_6$  as a function of temperature in a field of 2 T. Insets show (a) inverse susceptibility and (b) the inverse of the susceptibility with a constant offset,  $\chi_0$ , subtracted. Lines show fits to Curie-Weiss behavior. 'FU' refers to one formula unit.

ture (panel (a) of the inset to Fig. 5). Data between 75 and 200 K can nevertheless be fit by a Curie-Weiss law if a constant offset, attributed to Van Vleck paramagnetism, is included:  $\chi = C/(T - \theta) + \chi_0$  (panel (b) of the inset to Fig. 5). This fit results in effective moments  $\mu_{\text{eff}}$  of  $0.602(4)$ ,  $0.596(1)$ , and  $0.647(3) \mu_B$ , and Weiss temperatures of  $10(2)$ ,  $10(1)$ , and  $13(1)$  K for fields oriented in the [100], [111], and [110] directions respectively. Values of  $\chi_0$  are found to be  $3(1) \times 10^{-5}$ ,  $1.7(1) \times 10^{-4}$ , and  $1.76(9) \times 10^{-4} \text{ emu/mole}$  for fields oriented in these same directions.

The magnetic phase transition is most clearly seen in the heat capacity (Fig. 6). Data were taken using the relaxation method for 3-4 single crystals weighing a total of 2-3 mg, oriented at arbitrary angles to each other, for temperatures from 0.3 to 300 K. A sharp anomaly is seen with a peak at  $6.8(3)$  K, which defines the critical temperature  $T_c$ . The magnetic contribution to the heat capacity was estimated by subtracting a polynomial extrapolation of the higher temperature phonon heat capacity ( $C_{\text{ph}} = 0.065(7)T + 0.00262(6)T^3 - 2.6(1) \times 10^{-6}T^5$ , shown in Fig. 6). The total magnetic contribution to the entropy  $S_{\text{mag}}$  through this transition is found to be  $4.6 \text{ J/mole K}$  (right axis, Fig. 6), falling slightly short (80%) of  $R \ln 2 = 5.76 \text{ J/mole K}$ . This short-fall is attributed to systematic errors in the phonon subtraction, and the small amount of material used. No additional anomalies are observed up to 300 K (inset to Fig. 6).

The triply degenerate  $t_{2g}$  orbitals of  $\text{O}\text{SO}_6$  in the undistorted  $\text{Ba}_2\text{Na}_0.5\text{SO}_6$  crystal structure constitute an effective unquenched angular momentum  $L = 1$ . The ma-

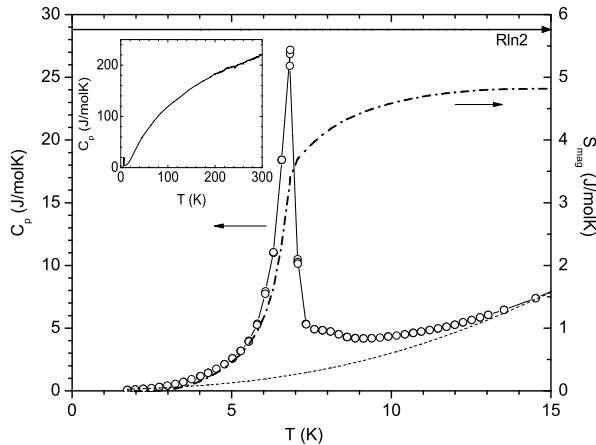


FIG. 6: Heat capacity (left axis) and magnetic contribution to the integrated entropy (right axis) for the magnetic transition in  $\text{Ba}_2\text{Na}_0\text{SO}_6$ . The dashed line (left axis) shows an extrapolation of a fit to the phonon background, the solid horizontal line (right axis) indicates the theoretical entropy of  $R \ln 2$  for a doublet groundstate. Inset shows the heat capacity to 300 K. Upper axis shows the Dulong-Petite value of 249 J/molK.

trix elements of the orbital angular momentum operator,  $L$ , within the  $t_{2g}$  manifold are the same as those of  $L$  within states of  $P$  symmetry [15]. Application of spin orbit coupling therefore results in a quartet ground state ( $J = 3/2$ ) and a doublet excited state ( $J = 1/2$ ) [15, 16]. Since the integrated entropy through the magnetic phase transition is  $R \ln 2$  we can surmise that the quartet must be split into two Kramers doublets at a temperature  $T_t > T_c$ .

The absence of a detectable structural distortion either above or below  $T_c$  rules out the usual mechanisms based on single ion anisotropy by which a weak ferromagnetic moment can be realized in a canted antiferromagnetic. Specifically, within the resolution of these measurements, the crystal lattice does not lose a center of inversion symmetry between the  $\text{O}$  ions, nor does it acquire sites with different uniaxial anisotropy. However, we note that ferromagnetism can arise naturally in a Mott insulator for which there is orbital degeneracy [17]. In such a scenario, antiferro-orbital ordering enables a gain in energy of ferromagnetic over antiferromagnetic superexchange due to the additional Hund's coupling. Such an effect is thought to account for the ferromagnetism in the  $3d^1$  material  $\text{YTIO}_3$  [9, 10]. In the case of  $\text{Ba}_2\text{Na}_0\text{SO}_6$ , the observation of a doublet ground state certainly indicates that the orbital degeneracy has been lifted, whilst the absence of any additional features in the heat capacity implies that  $T_t > 300$  K.

In the absence of measurements that probe the nature

of the orbital ordering in  $\text{Ba}_2\text{Na}_0\text{SO}_6$  we can only speculate as to the cause of the dramatic difference between them magnetic properties of this compound and the isostructural antiferromagnetic analog  $\text{Ba}_2\text{Li}\text{IO}_6$  [5]. Within the scenario described above, the Jahn-Teller distortion in these two compounds must be very different. The antiferromagnetic Mott insulator  $\text{LaTiO}_3$  [18, 19] is perhaps analogous to  $\text{Ba}_2\text{Li}\text{IO}_6$ . At room temperature,  $\text{LaTiO}_3$  is isostructural and isostructural to the ferromagnetic Mott insulator  $\text{YTIO}_3$  described above, but the degeneracy of the  $t_{2g}$  orbitals is lifted by a substantial structural transition at the Neel temperature [19]. It is intriguing to think that a similarly complex interplay between spin and orbital order may be present in the  $5d^1$  Mott insulators  $\text{Ba}_2\text{Na}_0\text{SO}_6$  and  $\text{Ba}_2\text{Li}\text{IO}_6$ . These results warrant further investigation of the title compound via neutron and resonant x-ray scattering to determine the nature of the magnetic structure, orbital ordering and spin density distribution in the ordered state.

#### Acknowledgments

The authors thank R. M. Whittle, Z. Islam, D. Mandrus and A. Sleight for useful conversations. This work is supported by the DOE, Office of Basic Energy Sciences, under contract no. DE-AC02-76SF00515, and the NSF under grant no. DMR-0134613. The authors would also like to thank Prof. V. K. Pecharsky and Dr. Y. M. Udryk for using their Rigaku PXRD. A part of this work was carried out at the Ames Laboratory, which is operated for the US Department of Energy by Iowa State University under Contract No. W-7405-ENG-82.

- 
- [1] J. E. Gledhill, et. al., *Inorg. Chem.* 7, 2461 (1968).
  - [2] V. I. Belova and Y. K. Syrkin, *Zh. Neorgan. Khim.* 3, 2016 (1958).
  - [3] K. L. Chamberland, *Mat. Res. Bull.* 13, 1273 (1978).
  - [4] W. R. Gemmill, et. al., *Inorg. Chem.* 44, 2639 (2005).
  - [5] K. E. Stitzer, et. al., *Solid State Sciences* 4, 311 (2002).
  - [6] A. W. Sleight, et. al., *Inorg. Chem.* 1, 245 (1962).
  - [7] K. E. Stitzer, et. al., *Inorg. Chem.* 42, 947 (2003).
  - [8] T. Moriga, *Magnetism* (Academic Press, 1963), Vol 1, pp. 85-125.
  - [9] C. Ullrich, et. al., *Phys. Rev. Lett.* 89, 167202 (2002).
  - [10] R. Schmitz, et. al., *Ann. Phys.* 14, 626, 2005.
  - [11] XRD Single Crystal Software, Bruker Analytical X-ray Systems, Madison, USA (2002).
  - [12] B. A. Hunter, *IUCR Powder Diffraction* 22 (1997).
  - [13] J. Hancock, et. al., *Phys. Rev. B* 73, 125119 (2006).
  - [14] W. A. Harrison, *Elementary Electronic Structure* (World Scientific, 2004).
  - [15] J. B. Goodenough, *Phys. Rev.* 171, 466 (1968).
  - [16] K. W. H. Stevens, *Proc. R. Soc. London Series A* 219, 542 (1953).

- [17] K. I. Kugeland D. I. Khomskii, Soviet Physics JETP 37, 725 (1973).
- [18] M. Cwik, et. al., Phys. Rev. B 68, 060401 (2003).
- [19] M. Mochizuki and M. Imada, J. Phys. Soc. Japan 73, 1833 (2004).
- [20] The bare value for O s is -13.74 eV [14]. Charge transfer between O s and O results in a shift in energy which can be calculated in a self-consistent manner. The shift in energy in  $E_d(Os)$  is given by  $E = U_d Z_d$ , with  $U_d = 3.4$  eV [14] and  $Z_d = 0.76$ , from which  $E_d(Os) = -13.74 - (3.4 \cdot 0.76) = -16.32$  eV.
- [21] Since the O s d orbitals are much smaller than the 4-atom O p-orbital cluster associated with one  $t_{2g}$  molecular orbital, the dominant contributions to  $U$  will come from

the O s site. The antibonding orbital has only a weak polarization, characterized by  $p = 0.067$  [14], such that roughly half of the charge resides in the O s d-orbital and half in the 4-atom O p-orbital cluster.  $U$  will therefore contain contributions from the self-energy of the two half electrons on the O s site,  $\frac{1}{4}U_d$ ; the coulomb repulsion between the O s  $\frac{1}{2}e$  and the  $\frac{1}{2}e$  in the p-orbital cluster a distance  $d$  away,  $\frac{1}{4}e^2/d$ ; and the coulomb attraction between the O s  $\frac{1}{2}e$  and the positive charge on the electron-decay neighbor a distance  $r$  away,  $\frac{1}{2}e^2/r$ , where  $r = 2d$ . The resulting total contribution  $U = \frac{1}{4}U_d + \frac{1}{4}e^2/d + \frac{1}{2}e^2/r = 3.32$  eV.